

Spin-orbit-coupled spin-1 Bose-Einstein condensates confined in radially periodic potential

Ji Li(李吉), Tianchen He(何天琛, Jing Bai(白晶), Bin Liu(刘斌), and Huan-Yu Wang(王寰宇)
Citation: Chin. Phys. B, 2021, 30 (**3**): 030302. DOI: 10.1088/1674-1056/abc53e
Journal homepage: http://cpb.iphy.ac.cn; http://iopscience.iop.org/cpb

What follows is a list of articles you may be interested in

Ferromagnetic transition of a spin–orbit coupled dipolar Fermi gas at finite temperature

Xue-Jing Feng(冯雪景) and Lan Yin(尹澜)
Chin. Phys. B, 2020, 29 (**11**): 110306. DOI: 10.1088/1674-1056/aba9ca

Lattice configurations in spin-1 Bose–Einstein condensates with the SU(3) spin–orbit coupling

Ji-Guo Wang(王继国)†, Yue-Qing Li(李月晴), and Yu-Fei Dong(董雨菲)
Chin. Phys. B, 2020, 29 (**10**): 100304. DOI: 10.1088/1674-1056/abab72

Landau-like quantized levels of neutral atom induced by a dark-soliton shaped electric field

Yueming Wang(王月明), Zhen Jin(靳祯)
Chin. Phys. B, 2020, 29 (**1**): 010303. DOI: 10.1088/1674-1056/ab5938

SU(3) spin-orbit-coupled Bose-Einstein condensate confined in a harmonic plus quartic trap

Hao Li(李昊), Fanglin Chen(陈方林)
Chin. Phys. B, 2019, 28 (**7**): 070302. DOI: 10.1088/1674-1056/28/7/070302

Tunable ground-state solitons in spin-orbit coupling Bose-Einstein condensates in the presence of optical lattices

Huafeng Zhang(张华峰), Fang Chen(陈方), Chunchao Yu(郁春潮), Lihui Sun(孙利辉), Dahai Xu(徐大海)
Chin. Phys. B, 2017, 26 (**8**): 080304. DOI: 10.1088/1674-1056/26/8/080304

Spin–orbit-coupled spin-1 Bose–Einstein condensates confined in radially periodic potential*

Ji Li(李吉)[1], Tianchen He(何天琛)[1,†], Jing Bai(白晶)[1], Bin Liu(刘斌)[2], and Huan-Yu Wang(王寰宇)[3]

[1] *Department of Physics, Taiyuan Normal University, Jinzhong* 030619, *China*
[2] *Basic Teaching Department, Shanxi Institute of Energy, Jinzhong* 030600, *China*
[3] *Beijing National Laboratory for Condensed Matter Physics, Institute of Physics, Chinese Academy of Sciences, Beijing* 100190, *China*

(Received 7 August 2020; revised manuscript received 1 October 2020; accepted manuscript online 28 October 2020)

We investigate the ground states of spin-1 Bose–Einstein condensates (BECs) with spin–orbit coupling in a radially periodic potential by numerically solving the coupled Gross–Pitaevskii equations. In the radially periodic potential, we first demonstrate that spin–orbit-coupled antiferromagnetic BECs support a multiring petal phase. Polar–core vortex can be observed from phase profiles, which is manifested as circularly symmetric distribution. We further show that spin–orbit coupling can induce multiring soliton structure in ferromagnetic BECs. It is confirmed especially that the wave-function phase of the ring corresponding to uniform distribution satisfies the rotational symmetry, and the wave-function phase of the ring corresponding to partial splitting breaks the rotational symmetry. Adjusting the spin–orbit coupling strength can control the number of petal in antiferromagnetic BECs and the winding numbers of wave-function in ferromagnetic BECs. Finally, we discuss effects of spin-independent and spin-dependent interactions on the ground states.

Keywords: the spinor Bose–Einstein condensates, spin–orbit coupling, radially periodic potential

PACS: 03.75.Lm, 03.75.Mn, 67.85.Fg, 67.85.Hj **DOI:** 10.1088/1674-1056/abc53e

1. Introduction

The spins of the alkali-metal atoms are essentially free in an optical trap, which provides the possibility of studying condensates with a spin degree of freedom, the spinor Bose–Einstein condensates (BECs).[1–3] Spinor BECs have a new feature in which the order parameter is a vector rather than scalar quantity, which offers an ideal platform for probing many interesting topological excitations.[4–16] In terms of the interatomic interactions, one can observe matter-wave solitons in BECs.[6] Some researchers discussed the properties of quantum spin vortices in spinor BECs.[7–9] For the spinor BECs with rotation, it is found that there are coreless vortex, axisymmetric vortex, and nonaxisymmetric vortex in the system.[10,11] Mizushima *et al*. found singular vortex-lattice phases in rotating ferromagnetic BECs.[12] During dynamics of rotating spinor BECs, Ji *et al*. studied fractionalized half-quantum vortices in theory.[13] Subsequently, Seo *et al*. observed fractionalized half-quantum vortices in experiment.[14,15] In Rabi-coupled spinor BECs, the ground state can support skyrmionic vortex lattices.[16] In recent years, the research of spin–orbit (SO) coupling has been widely concerned in the field of condensed matter. However, the SO coupling is only slightly adjustable in materials due to the limitation of its own material parameters. The SO coupling in BECs can be controlled and tuned by using optical fields or a sequence of pulsed homogeneous magnetic fields.[17–29] The recent realization of SO coupling in BECs, owing to coupling between the spin and the center-of-mass motion of the atom, provides more possibilities to explore exotic novel quantum states.[30–36] Wang *et al*. found that SO coupling can induce plane wave and density stripe phases in BECs without external potential.[30] If the external potential is considered, new topological excitations will appear in the system, such as half-skyrmion,[31] fractionalized vortices,[32] skyrmion lattice,[33] the monopoles with the polar–core vortex.[34] In addition, the SO coupling can lead to the appearances of quantum quasicrystals in dipolar condensates.[36]

Recently, the impact of SO coupling on BECs in ring-shaped potentials has attracted considerable interest, due to the persistent flow states and symmetry-breaking phenomena being found.[37–43] Zhang *et al*. studied the ground state properties of two-component SO-coupled BECs in a toroidal trap and showed that the system exhibits a modified stripe, an alternately arranged stripe, and countercircling states.[40] Wang *et al*. further discussed ground state phases of the SO-coupled spinor BECs in the toroidal trap.[43] Especially intriguing is the impact of SO-coupling on BECs in radially periodic potential. Kartashov *et al*. studied two-component SO-coupled BECs in radially periodic potential and found that the system supports stable multiring solitons.[44] An immediate question is that, whether the SO coupling induces unknown types of

*Project supported by the Scientific and Technologial Innovation Program of the Higher Education Institutions in Shanxi Province, China (Grant Nos. 2019L0813, 2019L0785, and 2019L0808).

†Corresponding author. E-mail: tywlxdh@qq.com

© 2021 Chinese Physical Society and IOP Publishing Ltd

ground state phases in spin-1 BECs confined in a radially periodic potential.

In this work, we consider the SO-coupled spin-1 BECs confined in a radially periodic potential. We first demonstrate numerically that SO-coupled antiferromagnetic BECs confined in the radially periodic potential support a multiring petal phase. In this situation, we can observe polar–core vortex from phase profiles, which is manifested as circularly symmetric distribution. Meanwhile, the number of petal in the system can be controlled by changing the SO coupling strength. Next, we show that SO coupling can induce multiring soliton structure in ferromagnetic BECs in the presence of the radially periodic potential. It is confirmed especially that the wave-function phase of the ring corresponding to uniform distribution satisfies the rotational symmetry, and the wave-function phase of the ring corresponding to partial splitting breaks the rotational symmetry. For the case of ferromagnetic BECs, it is also found that the SO coupling can control the winding numbers of wave-function corresponding to each component. Furthermore, we investigate the effect of spin-dependent interaction on the ground state. The results show that adjusting antiferromagnetic spin-dependent interaction can control symmetry of the petal structure, and increasing ferromagnetic spin-dependent interaction makes the condensation tend to the uniform distribution. Finally, we also discuss the ground state properties under different spin-independent interactions for a given spin-dependent interaction parameter. Our findings open new directions for the studies of topological defects in SO-coupled quantum systems confined in a radially periodic potential.

2. Model and basic equations

We consider the two-dimensional spin-1 BECs with a Rashba SO coupling in the radially periodic potential. The mean-field Hamiltonian of this system is written as[13,34,35]

$$H=\int \mathrm{d}^2\boldsymbol{r}\Big\{\boldsymbol{\Psi}^{\dagger}\left(-\hbar^2\nabla^2/(2m)+V(\boldsymbol{r})+\mathcal{V}_{\mathrm{soc}}\right)\boldsymbol{\Psi} + \left(\frac{c_0}{2}n^2+\frac{c_2}{2}[(n_1-n_{-1})^2+2|\Psi_1^*\Psi_0+\Psi_0^*\Psi_{-1}|^2]\right)\Big\}, \quad (1)$$

where $\boldsymbol{\Psi}=[\Psi_1(\boldsymbol{r}),\Psi_0(\boldsymbol{r}),\Psi_{-1}(\boldsymbol{r})]^{\mathrm{T}}$ (the superscript T stands for the transpose) is the order parameter of the BECs with normalization $\int\boldsymbol{\Psi}^{\dagger}\boldsymbol{\Psi}\,\mathrm{d}^2\boldsymbol{r}=N$, and N stands for the total particle number. The total particle density is represented as $n=\sum_m n_m$, wherein $n_m=|\boldsymbol{\Psi}_m(\boldsymbol{r})|^2$ with $m=0,\pm1$. In the kinetic term, m is the mass of ^{87}Rb atom and $\hbar$ is the Planck constant. $V(\boldsymbol{r})=2V_0\cos^2(r)$ indicates the radially periodic potential with depth $2V_0$. This potential can be created by using the cylindrical laser beam whose amplitude is modulated.[44,45] The SO coupling term is written as $\mathcal{V}_{\mathrm{so}}=-\mathrm{i}\hbar(\kappa_x\mathcal{F}_x\partial_x+\kappa_y\mathcal{F}_y\partial_y)$, where κ_x and κ_y are the strengths of the SO coupling. We define $\kappa_x=\kappa_y=\kappa$ in the case of the isotropic SO coupling (Rashba-type) and $\kappa_x\neq\kappa_y$ in the case of the anisotropic SO coupling. This work mainly considers Rashba SO coupling. The vector of spin-1 matrices is defined by $\mathcal{F}=(\mathcal{F}_x,\mathcal{F}_y,\mathcal{F}_z)^{\mathrm{T}}$, wherein $\mathcal{F}_x$, $\mathcal{F}_y$, and $\mathcal{F}_z$ are the 3×3 Pauli matrices of the spin angular momentum operators. For the interaction terms, the coupling parameters are given by $c_0=4\pi\hbar^2(a_0+2a_2)/3m$ and $c_2=4\pi\hbar^2(a_2-a_0)/3m$, where $a_{0,2}$ are two-body s-wave scattering lengths for total spin $0,2$. The dynamics of wave functions are formulated as the dimensionless coupled Gross–Pitaevskii equations

$$\mathrm{i}\frac{\partial\psi_1}{\partial t}=\left(-\frac{1}{2}\nabla^2+V+\lambda_0\rho+\lambda_2(\rho_1+\rho_0-\rho_{-1})\right)\psi_1 +\kappa(-\mathrm{i}\partial_x-\partial_y)\psi_0+\lambda_2\psi_{-1}^*\psi_0^2, \quad (2)$$

$$\mathrm{i}\frac{\partial\psi_0}{\partial t}=\left(-\frac{1}{2}\nabla^2+V+\lambda_0\rho+\lambda_2(\rho_1+\rho_{-1})\right)\psi_0 +\kappa(-\mathrm{i}\partial_x+\partial_y)\psi_1+\kappa(-\mathrm{i}\partial_x-\partial_y)\psi_{-1} +2\lambda_2\psi_1\psi_{-1}\psi_0^*, \quad (3)$$

$$\mathrm{i}\frac{\partial\psi_{-1}}{\partial t}=\left(-\frac{1}{2}\nabla^2+V+\lambda_0\rho+\lambda_2(\rho_0+\rho_{-1}-\rho_1)\right)\psi_{-1} +\kappa(-\mathrm{i}\partial_x+\partial_y)\psi_0+\lambda_2\psi_1^*\psi_0^2, \quad (4)$$

where the dimensionless wave function $\psi_j=N^{-1/2}a_{\mathrm{h}}\Psi_j$ and the total condensate density $\rho=\rho_1+\rho_0+\rho_{-1}$ with $\rho_j=|\psi_j|^2$ $(j=1,0,-1)$. The dimensionless radially periodic potential $V=V'\cos^2(r)$, V' is the dimensionless depth of radially periodic potential. The dimensionless interaction strengths $\lambda_0=4\pi N(a_0+2a_2)/3a_{\mathrm{h}}$ and $\lambda_2=4\pi N(a_2-a_0)/3a_{\mathrm{h}}$. We choose $a_2=(100.4\pm0.1)a_{\mathrm{B}}$ for total spin channel $F_{\mathrm{total}}=2$ and $a_0=(101.8\pm0.2)a_{\mathrm{B}}$ for total spin channel $F_{\mathrm{total}}=0$, where a_{B} is the Bohr radius.[34] t and x, y are dimensionless time and spatial coordinates, scaled to characteristic time $\hbar/\varepsilon_0$ and spatial scale a_{h}, respectively, $\varepsilon_0=\hbar^2/ma_{\mathrm{h}}^2$ is characteristic energy, a_{h} is characteristic length. κ is the dimensionless strength of the SO coupling. The ground state wave function of the system is obtained by using the standard imaginary-time propagation methods.[34,35,40] Equations (2)–(4) by using the fourier spectrum method for the spatial discretization and the backward/forward Euler schemes of the linear/nonlinear terms for the time discretization. In all numerical simulations, the size of the computational grid is 240×240, corresponding to the field of view being 20×20 (a_{h}^2). We start with the normalized random number as the initial condition. A sufficiently large number of time steps are chosen, which guarantees that we have reached a steady state.

3. Results and discussion

3.1. SO-coupled antiferromagnetic BECs in the radially periodic potential

We first study the ground states of SO-coupled antiferromagnetic BECs in the radially periodic potential. To highlight

the effect of the SO coupling, we fix the radially periodic potential and other parameters of the system. Figure 1 shows particle density profile and phase distribution of the ground states under different SO coupling strengths. For small κ, the condensation of the innermost ring is a uniform distribution. The condensation of outer ring exhibits the periodic density modulation along the azimuthal direction, which is a multiring petal phase as shown in Fig. 1(a). As shown in density distributions of three components, the numbers of petals along the corresponding ring for each component are the same. In addition, the numbers of petals corresponding to the outer ring are more than those of the inner ring. From phase profiles we can observe polar–core vortex, which is manifested as circularly symmetric distribution. The structure of the polar–core vortex in terms of the individual spin components is as follows: a singly antivortex in the $m_{\rm F}=+1$ component, a singly vortex in the $m_{\rm F}=-1$ component, and no vortex in the $m_{\rm F}=0$ component.[7–12] When the SO coupling strength is further increased, the condensation of the innermost ring is split into petal structure. For the case of the outer ring, compared with the number of petal in Fig. 1(a), it is found that the numbers of petals in Fig. 1(b) significantly increase.

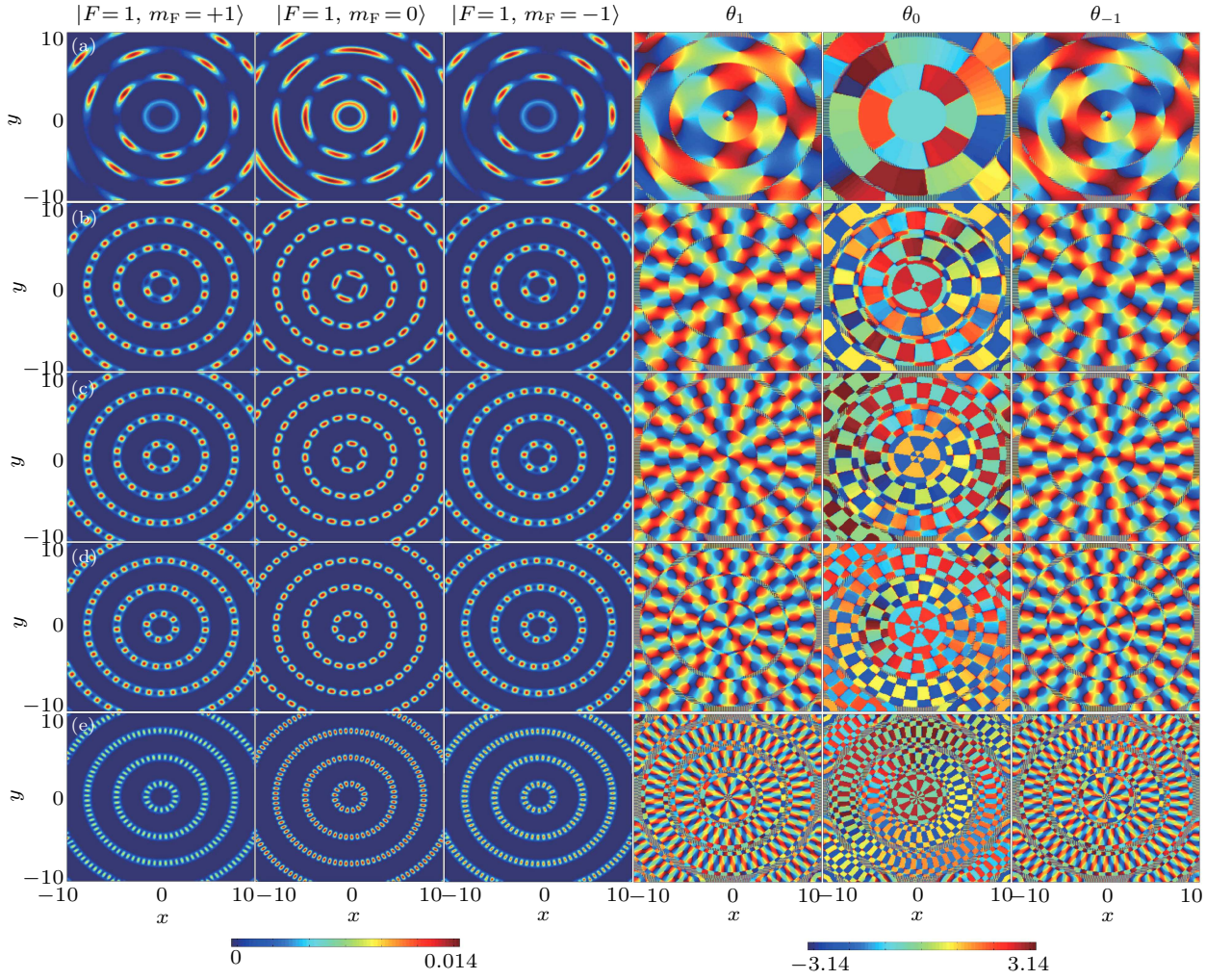


Fig. 1. Ground states of the antiferromagnetic BECs for the different SO coupling strengths in the radially periodic potential. In this situation, the SO coupling can induce multiring petal phase. The first, second, and third columns indicate the particle number densities. The fourth, fifth, and sixth columns indicate phase distributions. (a) $\kappa=0.4$; (b) $\kappa=1.2$; (c) $\kappa=1.6$; (d) $\kappa=2$; (e) $\kappa=4$. The rest of parameters are $\lambda_0=3200$, $\lambda_2=32$, and $V'=200$.

For even larger values of SO coupling, such as $\kappa=1.6,2$, the ground state remains multiring petal structure. The petal structure corresponding to the innermost ring will change from hexagonal symmetry arrangement shown in Fig. 1(c) to octagonal symmetry arrangement shown in Fig. 1(d). From Fig. 1(c) to Fig. 1(d) we also observe that the number of petal along outer ring gradually increase through enhancing the SO coupling. Next, we consider very strong SO coupling case as shown in Fig. 1(e), for example $\kappa=4$, the system always shows multiring petal phase, in which the number of petal reaches the maximum. Figure 1 confirms that the SO coupling can induce multiring petal phase in antiferromagnetic BECs in the presence of the radially periodic potential. As we all know that the SO coupling can induce stripe phase for the spinor BECs confined in harmonic trap.[30] In that situation the condensate density distributions show modified stripe

with single direction. In the present work, because of the radially periodic potential the density distributions will show modified stripe along the ring direction. Therefore the ground state is called the multiring petal phase. Meanwhile, the numbers of petals in the system can be controlled by changing the SO coupling strength. It is worth noting that we can observe polar–core vortex with circularly symmetric distribution in phase profiles. These intriguing phenomena can be understood by the fact that the rotational symmetry is broken, and on the other hand, SO coupling greatly changes the motion of atoms and the azimuthal motion in the radially periodic potential. To get a deeper physical insight into multiring petal phase in antiferromagnetic BECs, we take petal numbers of the innermost ring as an example. In Fig. 2, we plot the dependence of the petal numbers of the innermost ring on the SO coupling strength for fixed antiferromagnetic spin-dependent interaction. We find that the petal numbers can be controlled by adjusting the SO coupling strength. In addition, we also note that the petal numbers can display even or odd numbers. By comparing Figs. 2(a) and 2(c), the results show that the maximum number of petal becomes smaller when the antiferromagnetic spin-dependent interaction λ_2 is increased.

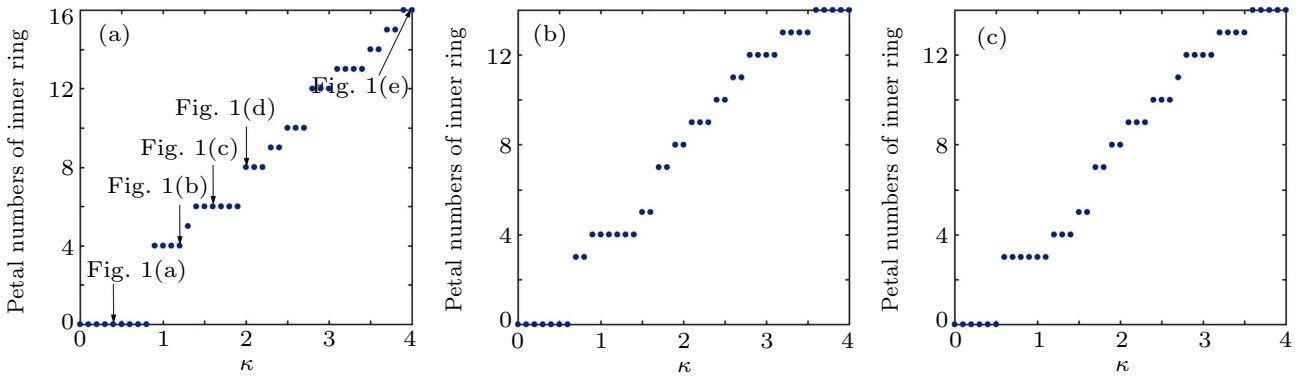


Fig. 2. Petal numbers of the inner ring as a function of the SO coupling strength for the antiferromagnetic BECs. (a) $\lambda_2 = 32$; (b) $\lambda_2 = 96$; (c) $\lambda_2 = 128$; Here $\lambda_0 = 3200$ and $V' = 200$.

3.2. SO-coupled ferromagnetic BECs in radially periodic potential

We next consider the SO-coupled ferromagnetic BECs in the radially periodic potential. Figure 3 shows particle density profiles and phase distribution of ferromagnetic BECs under different SO coupling strengths. From density profiles we can see that the ground state displays multiring soliton phase for the ferromagnetic BECs, as shown in the first three columns of Fig. 3. For small κ, it is found that there is phase separation between $m_F = +1$ component and $m_F = -1$ component, as shown in Fig. 3(a). The low density for $m_F = +1$ component is filled with $m_F = -1$ component. When the SO coupling is enhanced, such as $\kappa = 1.2$, the density of the innermost ring is a uniform distribution, as shown in Fig. 3(b). Meanwhile, the density of the outer ring is inhomogeneity distribution, which shows local splitting. For the case of phase profiles corresponding to the innermost ring, we can observe one-way circulating the wave-function phase with the rotational symmetry, which is similar to the plane wave.[30,40,43] More importantly, from the phase profiles of the innermost ring, one can see that there exists a winding number difference of one unit among different components,[41,43] which is highlighted by the black circle shown in Fig. 3(b). From the phase profiles of the outer ring, one can see that there exists circulating the wave-function phase with the rotational symmetry broken.

For even larger values of SO coupling, such as $\kappa = 1.6$, 2, and 4, the ground state always shows multiring soliton structure. It is worth noting that the condensation of the innermost ring presents a periodic splitting through increasing the strength of SO coupling, as shown in Figs. 3(c)–3(e), respectively. In addition, from the phase profiles of these ground states, one can see that the winding numbers of each component gradually increase with the increase of the SO coupling strength. Figure 3 confirms that the SO coupling can induce multiring soliton structure in ferromagnetic BECs in the presence of radially periodic potential. Meanwhile, increasing the strength of SO coupling can induce a periodic transition of the innermost ring from uniform distribution to partial splitting. Interestingly, it is also found that the wave-function phase of the ring corresponding to uniform distribution satisfies the rotational symmetry, and the wave-function phase of the ring corresponding to partial splitting breaks the rotational symmetry. In addition, we also demonstrate that the SO coupling can control the winding numbers of wave-function corresponding to each component. In order to see the multiring soliton structure more clearly, based on Figs. 3(b), 3(d), and 3(e), we plot the corresponding total particle number densities as shown in Fig. 4, which clearly shows the multiring soliton structure. From Fig. 3 we observe that the condensation density shows local splitting, which is caused by the phase separation among spin components.

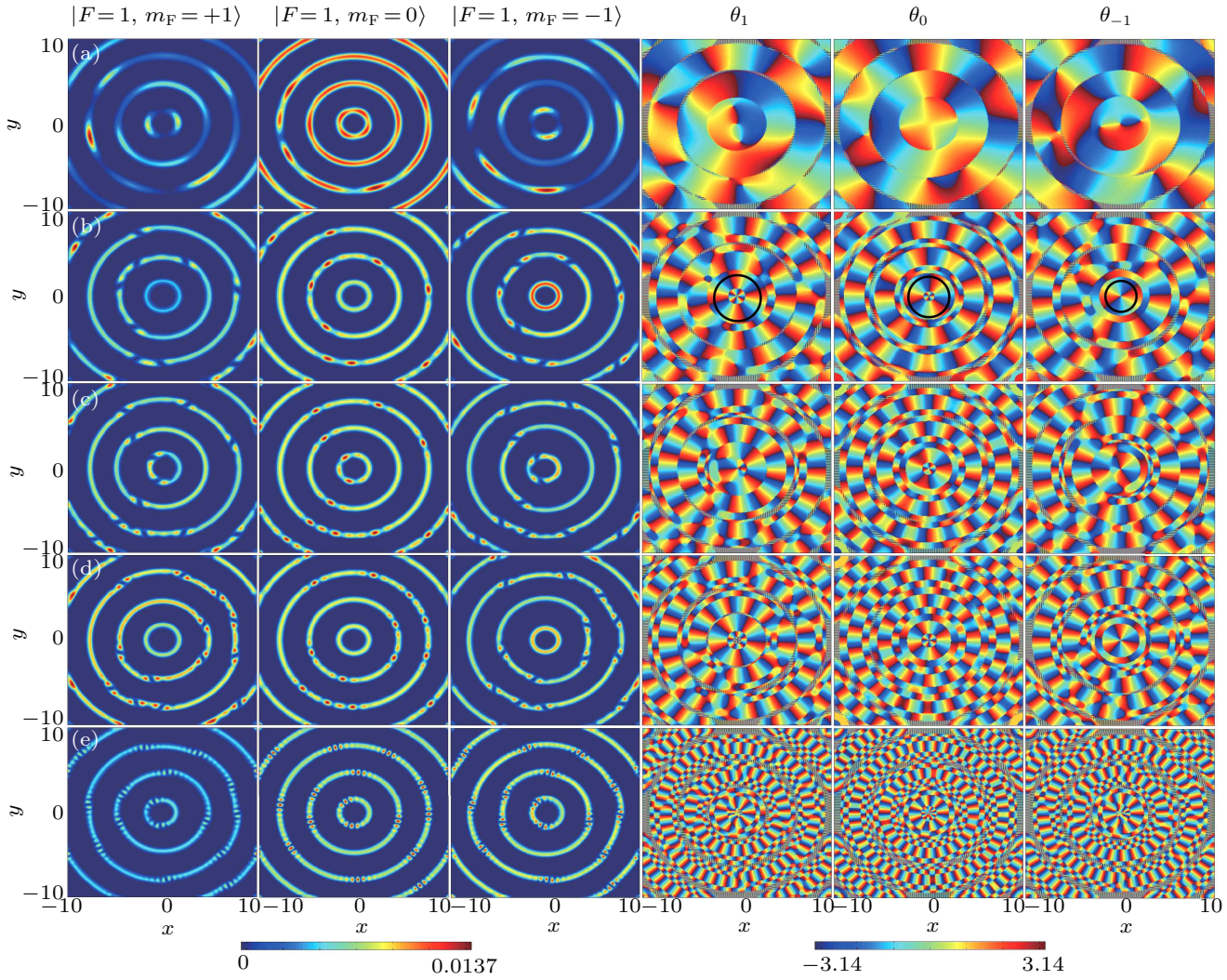


Fig. 3. Ground states of the ferromagnetic BECs for the different SO coupling strengths in the radially periodic potential. In this situation, the SO coupling can induce multiring soliton structure. The first, second, and third columns show the particle number densities. The fourth, fifth, and sixth columns show phase distributions. (a) $\kappa = 0.4$; (b) $\kappa = 1.2$; (c) $\kappa = 1.6$; (d) $\kappa = 2$; (e) $\kappa = 4$. The rest of parameters are $\lambda_0 = 3200$, $\lambda_2 = -32$, and $V' = 200$.

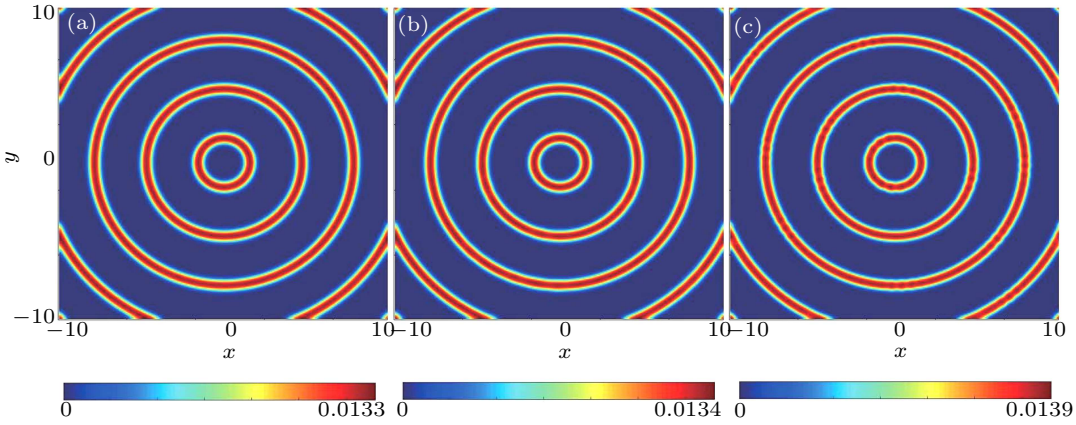


Fig. 4. Total particle number densities corresponding to the multiring soliton structure. (a) Total particle number densities corresponding to Fig. 3(b). (b) Total particle number densities corresponding to Fig. 3(d). (c) Total particle number densities corresponding to Fig. 3(e).

3.3. Effects of spin-independent and spin-dependent interactions on ground states

Now we turn to effects of spin-independent and spin-dependent interactions on the ground states. Figure 5 shows particle density profiles and phase distribution of the ground states under different antiferromagnetic spin-dependent interactions for a given spin-independent interaction parameter. When antiferromagnetic spin-dependent interaction $\lambda_2 = 12$, the ground state displays multiring petal phase as shown in Fig. 5(a). At the same time, the petal structure corresponding to the innermost ring displays quadrangular symmetry ar-

rangement. We also find the phase separation that is reflected in the densities of the $m_F = 0$ component and $m_F = \pm 1$ component. When the spin-dependent interaction is further increased, for example $\lambda_2 = 64, 128$, corresponding to Figs. 5(b) and 5(c), respectively, the numerical results show that adjusting antiferromagnetic spin-dependent interaction can control symmetry of the petal structure and the number of petal in every ring.

Figure 6 shows particle density profiles and phase distribution of the ground states under different ferromagnetic spin-dependent interactions for a given spin-independent interaction parameter. When ferromagnetic spin-dependent interaction $\lambda_2 = -12$, the ground state displays multiring soliton phase as shown in Fig. 6(a). From density profiles we also observe the phase separation between $m_F = 1$ component and $m_F = -1$ component. With the increase of spin-dependent interaction, for example $\lambda_2 = -64, -128$, the condensation of the innermost ring displays uniform distribution as shown in Figs. 6(b) and 6(c). For the case of outer ring, the condensation tends to the uniform distribution compared with Fig. 6(a). Figure 6 confirms that increasing ferromagnetic spin-dependent interaction leads to the uniform distribution of the condensation in the innermost ring. In addition, the condensation corresponding to the outer ring also tends to the uniform distribution.

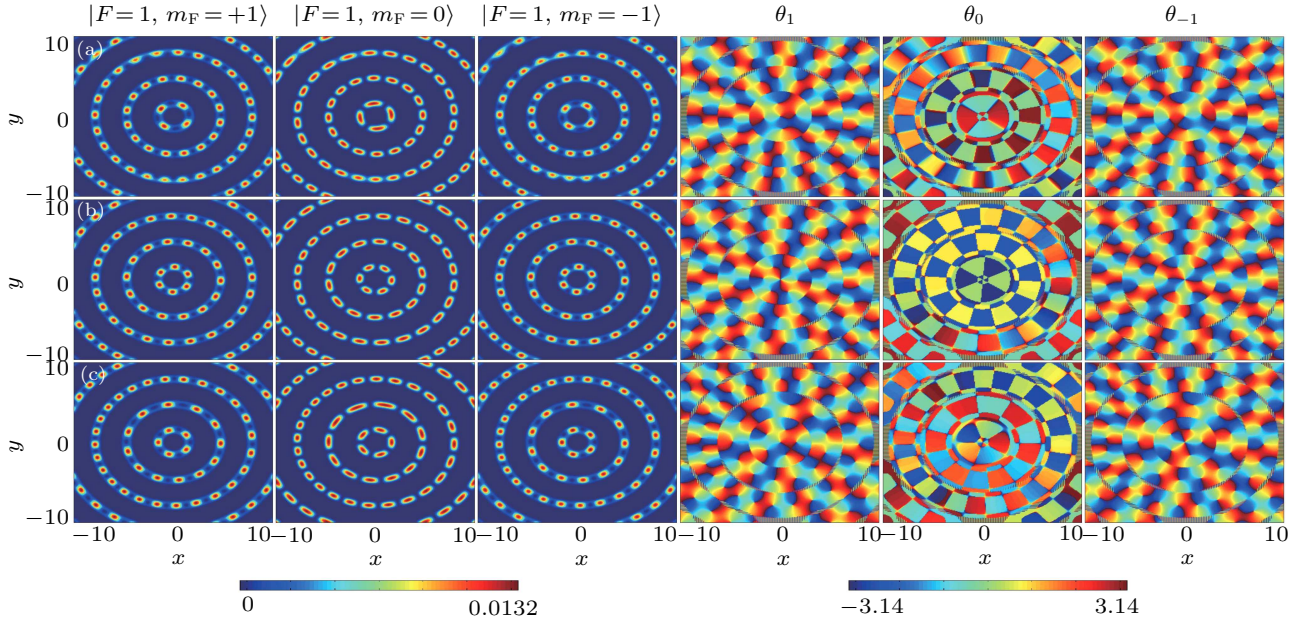


Fig. 5. Ground states under different antiferromagnetic spin-dependent interactions for a given spin-independent interaction parameter. (a) $\lambda_2 = 12$; (b) $\lambda_2 = 64$; (c) $\lambda_2 = 128$. The rest of parameters are $\lambda_0 = 3200$, $\kappa = 1.2$, and $V' = 200$.

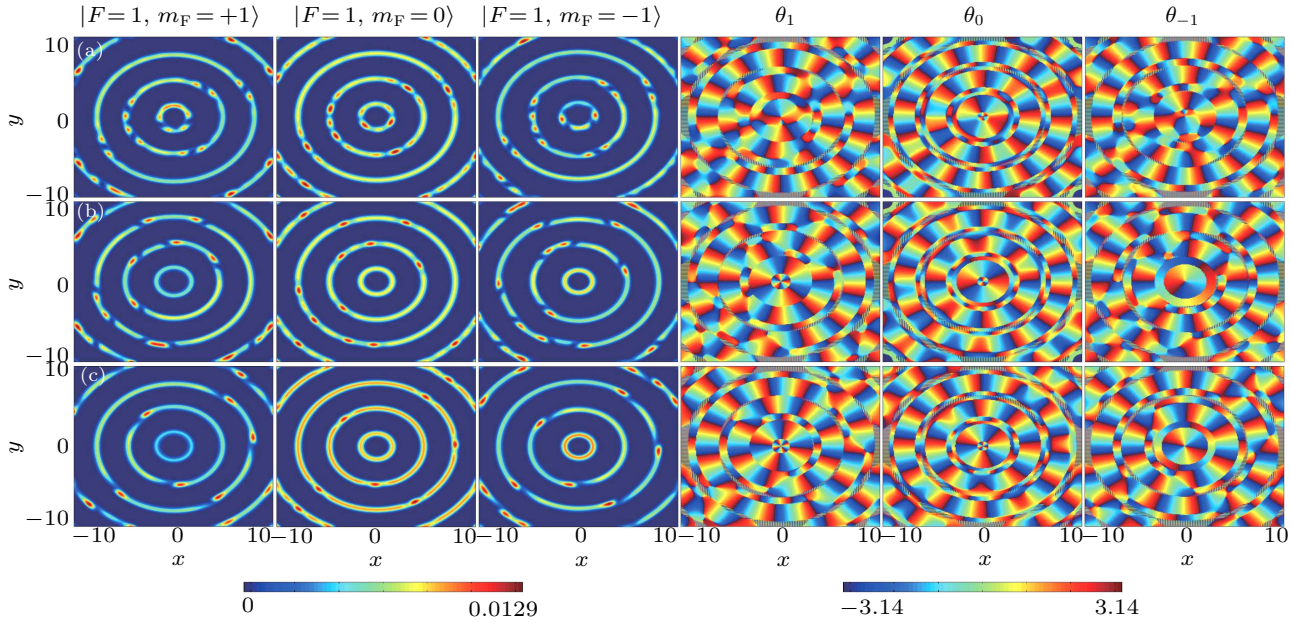


Fig. 6. Ground states under different ferromagnetic spin-dependent interactions for a given spin-independent interaction parameter. (a) $\lambda_2 = -12$; (b) $\lambda_2 = -64$; (c) $\lambda_2 = -128$. The rest of parameters are $\lambda_0 = 3200$, $\kappa = 1.2$, and $V' = 200$.

In Fig. 7, we discuss the ground state properties under different spin-independent interactions for a given spin-dependent interaction parameter. For a given antiferromagnetic spin-dependent interaction parameter, such as $\lambda_2 = 32$, the results show that the ground states always show the multiring petal phase with symmetry arrangement as the spin-independent interaction is enhanced. The numbers of petals on each ring are almost unchanged. Increasing spin-independent interaction can induce the increase of the number of particles in the system, which only leads to the increase of the distribution area corresponding to the petal as shown in Fig. 7(a1) and Fig. 7(a2). For a given ferromagnetic spin-dependent interaction parameter, such as $\lambda_2 = -32$, the results show that the ground states always show the multiring soliton phase as the spin-independent interaction is enhanced. It is easy to see that the condensation of the innermost ring shows inhomogeneity distribution for very strong spin-independent interaction as shown in Fig. 7(b2). In fact, the interactions can cause the variation of the local magnetic order,[5,34] leading to the interesting phenomenon shown in Figs. 5–7. Finally, we plot the dependence of the chemical potential on the strength of the SO coupling for the antiferromagnetic and ferromagnetic BECs as shown in Fig. 8. It can be seen that the chemical potential is increasing with the SO coupling. From Fig. 8(a) we find that the multiring petal phase in Fig. 1(a) is smoothly changed to the phase in Fig. 1(e) as κ is increased. The multiring soliton phase corresponding to Fig. 3 is highlighted by the black arrow in Fig. 8(b).

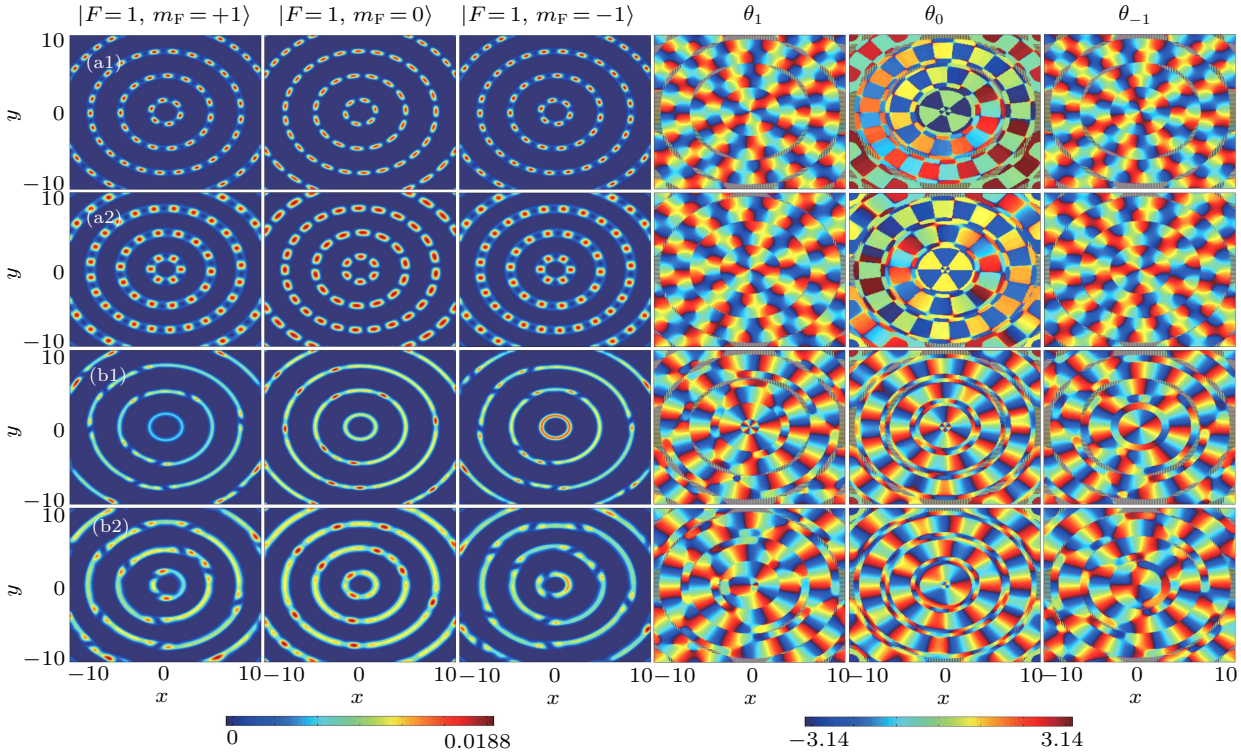


Fig. 7. Ground states properties under different spin-independent interactions for a given spin-dependent interaction parameter. (a1) $\lambda_2 = 32$, $\lambda_0 = 1200$; (a2) $\lambda_2 = 32$, $\lambda_0 = 6400$; (b1) $\lambda_2 = -32$, $\lambda_0 = 1200$; (b2) $\lambda_2 = -32$, $\lambda_0 = 6400$. The rest of parameters are $\kappa = 1.2$ and $V' = 200$.

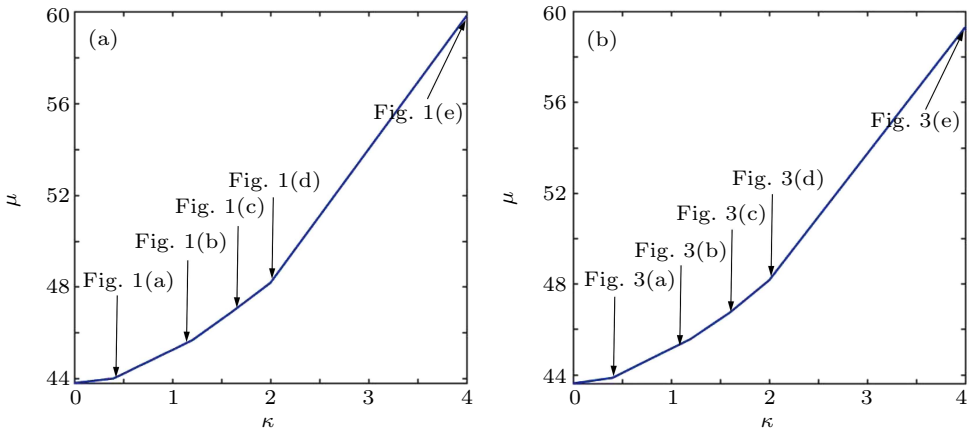


Fig. 8. (a) Chemical potential μ as a function of the SO coupling strength κ for the antiferromagnetic BECs. The multiring petal phase Fig. 1(a) is smoothly changed to the phase Fig. 1(e) as κ is increased. Here $\lambda_0 = 3200$ and $\lambda_2 = 32$. (b) Chemical potential μ as a function of the SO couplig strength κ for the ferromagnetic BECs. The multiring soliton phase corresponding to Fig. 3 is highlighted by the black arrow. Here $\lambda_0 = 3200$ and $\lambda_2 = -32$.

4. Conclusion

In conclusion, we have investigated the ground states of SO-coupled BECs confined in the radially periodic potential. For the antiferromagnetic BECs, we have demonstrated that the SO coupling can induce the multiring petal phase. The polar–core vortex was found in phase profiles, which is manifested as circularly symmetric distribution. For the ferromagnetic BECs, it was found that the SO coupling can induce multiring soliton structure. Especially, it was confirmed that the wave-function phase of the ring corresponding to uniform distribution satisfies the rotational symmetry, and the wave-function phase of the ring corresponding to partial splitting breaks the rotational symmetry. We have shown that adjusting the SO coupling strength can control the number of petal in antiferromagnetic BECs and the winding numbers of wave-function in ferromagnetic BECs. The influences of the interactions on the properties of the ground states have also been investigated. This work provides the basis for further investigations of the quantum system with the high-dimensional SO coupling[46] in the presence of the radially periodic potential.

References

[1] Ho T L 1998 *Phys. Rev. Lett.* **81** 742
[2] Klausen N N, Bohn J L and Greene C H 2001 *Phys. Rev. A* **64** 053602
[3] Görlitz A, Gustavson T L, Leanhardt A E, Löw R, Chikkatur A P, Gupta S, Inouye S, Pritchard D E and Ketterle W 2003 *Phys. Rev. Lett.* **90** 090401
[4] Bloch I, Dalibard J and Zwerger W 2008 *Rev. Mod. Phys.* **80** 885
[5] Stamper-Kurn D M and Ueda M 2013 *Rev. Mod. Phys.* **85** 1191
[6] Li L, Li Z D, Malomed B A, Mihalache D and Liu W M 2005 *Phys. Rev. A* **72** 033611
[7] Isoshima T, Machida K and Ohmi T 2001 *J. Phys. Soc. Jpn.* **70** 1604
[8] Tuchiya S J and Kurihara S 2001 *J. Phys. Soc. Jpn.* **70** 1182
[9] Kasamatsu K, Tsubota M and Ueda M 2005 *Int. J. Mod. Phys. B* **19** 1835
[10] Mizushima T, Machida K and Kita T 2002 *Phys. Rev. A* **66** 053610
[11] Martikainen J P, Collin A and Suominen K A 2002 *Phys. Rev. A* **66** 053604
[12] Mizushima T, Kobayashi N and Machida K 2004 *Phys. Rev. A* **70** 043613
[13] Ji A C, Liu W M, Song J L and Zhou F 2008 *Phys. Rev. Lett.* **101** 010402
[14] Seo S W, Kang S J, Kwon W J and Shin Y 2015 *Phys. Rev. Lett.* **115** 015301
[15] Seo S W, Kwon W J, Kang S J and Shin Y 2016 *Phys. Rev. Lett.* **116** 185301
[16] Orlova N V, Kuopanportti P and MiloševićM V 2016 *Phys. Rev. A* **94** 023617
[17] Lin Y J, Jiménez-García K and Spielman I B 2011 *Nature* **471** 83
[18] Ji S C, Zhang J Y, Zhang L, Du Z D, Zheng W, Deng Y J, Zhai H, Chen S and Pan J W 2014 *Nat. Phys.* **10** 314
[19] Wu Z, Zhang L, Sun W, 1 Xu X T, Wang B Z, Ji S C, Deng Y J, Chen S, Liu X J and Pan J W 2016 *Science* **354** 83
[20] Huang L H, Meng Z M, Wang P J, Peng P, Zhang S L, Chen L C, Li D H, Zhou Q and Zhang J 2016 *Nat. Phys.* **12** 540
[21] Wang P J, Yu Z Q, Fu Z K, Miao J, Huang L H, Chai S J, Zhai H and Zhang J 2012 *Phys. Rev. Lett.* **109** 095301
[22] Campbell D L, Juzeliúnas G and Spielman I B 2011 *Phys. Rev. A* **84** 025602
[23] Zhang J Y, Ji S C, Chen Z, Zhang L, Du Z D, Yan B, Pan J S, Zhao B, Deng Y J, Zhai H, Chen S and Pan J W 2012 *Phys. Rev. Lett.* **109** 115301
[24] Liu X J, Borunda M F, Liu X and Sinova J 2009 *Phys. Rev. Lett.* **102** 046402
[25] Anderson B M, Spielman I B and Juzeliúnas G 2013 *Phys. Rev. Lett.* **111** 125301
[26] Anderson B M, Juzeliúnas G, Galitski V M and Spielman I B 2012 *Phys. Rev. Lett.* **108** 235301
[27] Cheuk L W, Sommer A T, Hadzibabic Z, Yefsah T, Bakr W S and Zwierlein M W 2012 *Phys. Rev. Lett.* **109** 095302
[28] Ruseckas J, Juzeliúnas G, Öhberg P and Fleischhauer M 2005 *Phys. Rev. Lett.* **95** 010404
[29] Lan Z H and Öhberg P 2014 *Phys. Rev. A* **89** 023630
[30] Wang C J, Gao C, Jian C M and Zhai H 2010 *Phys. Rev. Lett.* **105** 160403
[31] Su S W, Liu I K, Tsai Y C, Liu W M and Gou S C 2012 *Phys. Rev. A* **86** 023601
[32] Sinha S, Nath R and Santos L 2011 *Phys. Rev. Lett.* **107** 270401
[33] Hu H, Ramachandhran B, Pu H and Liu X J 2012 *Phys. Rev. Lett.* **108** 010402
[34] Li J, Yu Y M, Zhuang L and Liu W M 2017 *Phys. Rev. A* **95** 043633
[35] Li J, Zhang X F and Liu W M 2018 *Ann. Phys.-New York* **396** 87
[36] Gopalakrishnan S, Martin I and Demler E A 2013 *Phys. Rev. Lett.* **111** 185304
[37] Mason P and Berloff N G 2009 *Phys. Rev. A* **79** 043620
[38] Ryu C, Andersen M F, Cladé P, Natarajan V, Helmerson K and Phillips W D 2007 *Phys. Rev. Lett.* **99** 260401
[39] Abad M, Guilleumas M, Mayol R and Pi M 2010 *Phys. Rev. A* **81** 043619
[40] Zhang X F, Kato M, Han W, Zhang S G and Saito H 2017 *Phys. Rev. A* **95** 033620
[41] White A C, Zhang Y P and Busch T 2017 *Phys. Rev. A* **95** 041604(R)
[42] Karabulut E Ö, Malet F, Fetter A L, Kavoulakis G M and Reimann S M 2016 *New J. Phys.* **18** 015013
[43] Wang J G, Xu L L and Yang S J 2017 *Phys. Rev. A* **96** 033629
[44] Kartashov Y V and Zezyulin D A 2019 *Phys. Rev. Lett.* **122** 123201
[45] Baizakov B B, Malomed B A and Salerno M 2006 *Phys. Rev. E* **74** 066615
[46] Song S W, Sun R, Zhao H, Wang X and Han B Z 2016 *Chin. Phys. B* **25** 040305